Polish J. Chem., **78**, 1327–1337 (2004)

Electrochemical Synthesis and Properties of Micro- and Nanocrystallites of Cobalt*

by A. Wiśniewski, P. Paklepa and P.K. Wrona**

Department of Chemistry, University of Warsaw, Pasteura 1, 02-093 Warsaw, Poland

(Received March 11th, 2004; revised manuscript June 7th, 2004)

The electrochemical synthesis of cobalt particles has been performed by electroreduction of Co(II) ions on the mercury electrode at potentials about –1.4 V *vs*. SCE. The electroreduction of Co(II) observed in cyclic voltammetry (CV), was a totally irreversible process due to the formation of an unstable cobalt amalgam, which decomposed into metallic cobalt. It has also been observed that metallic cobalt, practically insoluble in mercury, tends to aggregate, forming nanocrystallites and clusters that finally separate from mercury in the form of a black powder. The black cobalt powder, obtained this way, has been characterized using scanning electron microscope (SEM) imaging, X-ray analysis and specific surface measurements (nitrogen adsorption according to BET isotherm). The results of these experiments indicate that the cobalt powder obtained from the amalgam consists of partially oxidized crystallites of dimensions less than 20 nm. These nanocrystallites form aggregates of dimensions up to several or more μm. Due to their specific surface exceeding 30 m^2/g, such crystallites can be used for the preparation of metallic catalysts. A hypothesis, concerning the nucleation and further aggregation of Co from a homogeneous cobalt amalgam, leading to the formation of nanocrystallites, is discussed according to the burst-nucleation theory.

Key words: heterogeneous cobalt amalgam, nanocrystallites, voltammetry, specific surface measurements, BET isotherm, XRD analysis of powders, cobalt catalysts, nucleation, growth theory

Cobalt nanocrystallites and nanoparticles can be prepared using various methods, *e.g*. cobalt carbonyl pyrolysis [1,2], decomposition or reduction of other metal-containing compounds [3,4], atomic beam deposition, and some other physical and chemical methods [1,5]. Also, electrochemical generation of metallic particles from amalgams can be used as a method for obtaining crystallites, for example cobalt and iron [6,7]. The processes involving preparation and decomposition of cobalt and iron amalgams are of great importance due to the possibilities of technical applications of both amalgams and the nanocrystallites including liquid magnets, cobalt-based catalysts, fuel cell electrodes and, recently, enhancement of Ni-H cells properties by cobalt powder addition [8,9].

Usually, during the electroreduction of Co^{2+} on the Hg electrode, the microcrystals of Co in the mercury phase are formed and the formation of a homogeneous cobalt amalgam is not observed [10]. However, at low temperatures and concentrations

* Dedicated to Prof. Dr. Z. Galus on the occasion of his 70th birthday.

** Corresponding author. Email address: albin@chem.uw.edu.pl

of Co^{2+}, an oxidation of homogeneous, supersaturated cobalt amalgam can be seen [11]. Similarly, the oxidation of chromium amalgam is possible, if the experiments are carried out in the millisecond time scale [12], especially at low temperatures [13]. The electrochemical formation and decomposition of cobalt and chromium amalgams have been studied [11], using cyclic voltammetry (CV) and double potential step chronocoulometry (DPSC). In a short time (milliseconds) after the formation of the homogeneous amalgam, the unusual changes in the chronocoulometric curves suggested the formation of small metallic clusters (probably dimers or trimers) [11,13]. This phenomenon can be associated with low solubilities of Co and Cr in Hg (below the detection limit of 10^{-5} at. %) [14].

The growth mechanism of magnetic particles (iron and cobalt) in the mercury phase has been discussed by Luborsky [15] and Windle *et al*. [7]. In another paper by Luborsky [16], it has been stated that very small, about 2 nm, iron particles form a gel-like mixture, in which each particle is surrounded by mercury. This dispersion is quite stable for hours, but the particles grow slowly and finally leave the mercury phase. The growth of iron particles starting with metallic nuclei in mercury has been explained according to the Thomson-Freundlich relation. Since small particles are more easily soluble than bigger ones (equilibrium concentration of a solute for the smaller particles is higher), the process of Fe growth initially proceeds with the dissolution of smaller particles, than the diffusion of iron through mercury, and, finally, the growth of the larger iron particles. However, the Fe growth mechanism is still not well understood. For example, according to the same paper, there is no evidence of coagulation followed by recrystallization in the growth process, because mercury adsorbed on the surface of the particles should prevent the actual collision of two particles. On the contrary, other authors [7] claim that clustering of particles begins due to the magnetic interactions between single particles and that the particles within the cluster still grow by diffusion. It is also possible [17,18] to inhibit the growth of the metallic particles by the addition of metals like tin and gallium, which cover iron or cobalt particles.

One of the most important parameters describing nanocrystallites is their size. Because magnetic properties of nanocrystallites are strongly related to their dimensions, methods usually used for size determination include: magnetization, coercive force and the remanence measurements [6]. For spherical cobalt particles the magnetic domains appear when the radius of the sphere is about 35 nm [5]. For smaller superparamagnetic cobalt nanoparticles, ferromagnetic resonance can also be used [4]. Some other methods of crystallite size determination are based on tin adsorption, electron micrographs and growth kinetics [6]. Also, an X-ray diffraction seems to be a useful method for nanoparticle size determination. For example, Puntes *et al*. [1] calculated from the peak broadening of the revealed X-ray diffraction pattern, an average crystal size of 9.1 nm of the particles obtained by the decomposition of $Co_2(CO)_8$. Also Diehl *et al*. [4] used X-ray powder diffraction to confirm structural parameters of Co nanoparticles using numerical methods to calculate the actual size of the particles by the X-ray diffraction pattern simulation.

Very small cobalt particles are readily oxidized [2]. For example Diehl *et al*. [4] found that nanoparticles are covered by *ca*. 0.5 nm deep oxide layer. Also, from our earlier observations concerning the decomposition of amalgams (especially chromium amalgam) [11,12] we have deduced that the nanocrystallites, characterized by highly developed surface and high activity, are not chemically stable in aqueous and air environment. For example, chromium obtained that way exhibits pyrophoric properties [11].

In this work, we decided to decompose the cobalt amalgam under non-aqueous solvent to slow down the oxidation of crystallites. Such a layer of organic solvent should also limit the contact of the crystallites with the atmospheric oxygen, thus at least partially preventing the oxygenation of the metallic particles. We also investigated the effect of the concentration of Co atoms in mercury, *i.e*. the amount of Co(II) reduced into the mercury phase, on the formation of Co nanocrystallites. As shown before [6], during the reduction of cobalt ions on the mercury electrode, minimal particle sizes are obtained at low current densities related to lower Co concentration in mercury. We decided therefore to investigate the effect of the concentration of cobalt in the amalgam on the properties of the cobalt powder. We were curious to what extent one can change cobalt nanocrystallites properties by changing the cobalt concentration in mercury. For this purpose we prepared cobalt amalgams with various cobalt concentrations and, after separation of cobalt powder, we measured the parameters of nanocrystallites using various methods. The results are discussed according to various microcrystallites growth theories.

EXPERIMENTAL

Materials and apparatus. $Co(ClO_4)_2 \cdot 6\ H_2O$ (p.a.) produced by Ventron was used without further purification to obtain approx. 0.1 M $Co(ClO_4)_2$ aqueous solution. Acetone (p.a.) and hexane (p.a.) provided by POCh (Gliwice, Poland) were used without further purification. Chemically pre-treated and triply distilled mercury and MilliQ water (distilled twice before purification) were used in the experiments. The electrolysis of Co^{2+} ions on mercury pool electrode was conducted with EG&G Model 366A Bi-potentiostat. In the experiments, a constant volume (10 ml) of mercury, placed on the bottom of the electrochemical cell, served as a cathode in the deposition experiments (*ca*. 7 cm^2 surface area). As an anode, a platinum plate with high area, separated from the electrochemical cell by the glass frit, was used. As a reference electrode, saturated calomel electrode (SCE) was applied. The real surface measurements were conducted on Gemini 2370 V3.02 apparatus using the method based on nitrogen adsorption according to BET (Brunauer, Emmett, Teller) isotherm. Nanocrystallites in the form of powders have been analysed using X-ray diffraction in measurement mode θ-2θ and Bragg-Brentano geometry using filtered radiation Fe Kα of the wavelength equal to 0.19373 nm.

RESULTS AND DISCUSSION

Preparation of cobalt amalgams and cobalt nanocrystallites. Initially, the cyclic voltammetric curves of Co^{2+}/Co(Hg) redox system were recorded in order to determine the appropriate conditions for the bulk electrolysis of Co^{2+}. The solution contained 1 mM Co^{2+} in unbuffered supporting electrolyte (0.1 M $NaClO_4$). The range of scan rates applied was from 0.01 to 0.1 V/s (Fig. 1).

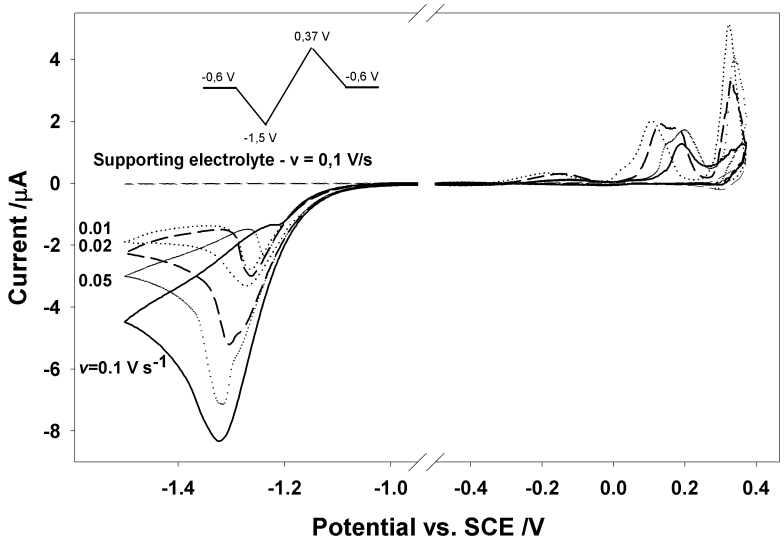

Figure 1. Cyclic voltammetric (CV) curves of Co^{2+} reduction and Co amalgam oxidation on HMDE in 0.1 M $NaClO_4$ solution containing 1 mM Co^{2+}.

The voltammetric curves in Fig. 1 show that the Co (II) /Co(Hg) redox reaction is totally irreversible under the conditions of the experiment, because the difference between cathodic and anodic peak potentials is greater than 1 V. From the irregular shapes of the anodic and cathodic curves, one can deduce that both processes, the reduction of Co^{2+} and the oxidation of Co from mercury, are complex. The reasons for such a behaviour, presented in our earlier paper [11], are as follows: (a) in the potential range from –0.2 to 0.4 V, we probably do not observe the oxidation of homogeneous cobalt amalgam, as it decomposes too fast to be seen with the CV technique, but another forms of metallic cobalt are oxidized to Co(II) and Co(III); (b) the irregularities on the anodic curves are probably a result of an increased pH in the vicinity of the electrode causing the oxidation of Co(II) to Co(III) hydroxide in an unbuffered solution; and (c) in the case of cathodic curves the irregularities result probably from hydrogen evolution reaction (HER) catalysis by cobalt nanocrystallites protruding from the mercury surface.

Since the electroreduction peak of Co^{2+} ions appears on CV curves from about –1.20 V to –1.35 V, depending on the potential scan rate, we decided to conduct the electrolysis of Co^{2+} on a mercury pool cathode at a constant potential of –1.45 V *vs.* SCE at room temperature. To prepare the nanocrystallites, the Co^{2+} solution was regularly changed when exhausted in cobalt ions, and the reduction was conducted until the concentration of cobalt in mercury reached a defined level. The exhaustion of the solution in Co^{2+} ions was recognized visually and confirmed spectrophotometrically. The volume of each portion of 0.1 M Co^{2+} solution was equal to 25 ml. In the calculation of the amalgam concentration it was assumed that all cobalt Co^{2+} from the solution was reduced into a known amount of mercury, forming cobalt amalgam.

The cobalt amalgam obtained as described above was flushed with water, then with acetone and hexane, and stored under hexane. With high cobalt concentrations in the amalgam used in this work, the separation of metallic cobalt was visible after less than one hour, starting from the time of disconnecting the circuit. The mercury surface became dull and a slow separation of crystallites started. The samples of cobalt crystallites were obtained as a hexane suspension after 1–2 weeks. All the operations were conducted in air, *i.e*. the suspensions in organic solvents were not isolated from the atmospheric oxygen. In SEM imaging, the suspension was used directly, otherwise hexane was evaporated to obtain cobalt powder.

The experiments, which differed in Co concentration and mode of stirring (mechanical or magnetic stirrer) were carried out as described below:

(i) *Cobalt 0* – a sample prepared from amalgam with concentration of cobalt in mercury *ca*. 6.7 at. %, stirred with a magnetic stirrer.

(ii) *Cobalt 1* – a sample prepared from amalgam with concentration of cobalt in mercury *ca*. 6.52 at. %, stirred with a mechanical stirrer.

(iii) *Cobalt 2* – a sample prepared from amalgam with concentration of cobalt in mercury *ca*. 1.36 at. %, stirred with a mechanical stirrer.

These samples have been analysed using various methods: SEM, BET and X-ray diffraction.

SEM images of cobalt nanocrystallites. In Fig. 2 a general view of Co crystallites at low magnification is presented. The crystallites (agglomerates) are not uniform and their size is in the range of microns.

In the SEM images presented in Fig. 3 and 4, the same magnification was used. The first image (Fig. 3) shows cobalt nanocrystallites obtained from the amalgam having higher concentration (6.52 at. %, Cobalt 1) than in Fig. 4 (1.36 at. %, Cobalt 2).

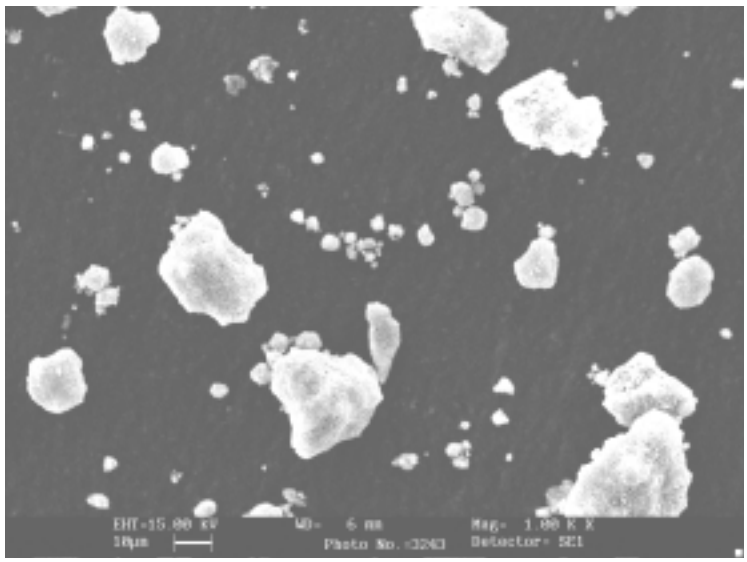

Figure 2. The SEM image at low magnification (1000 x) of the crystallites obtained from 6.52 at. % Co amalgam.

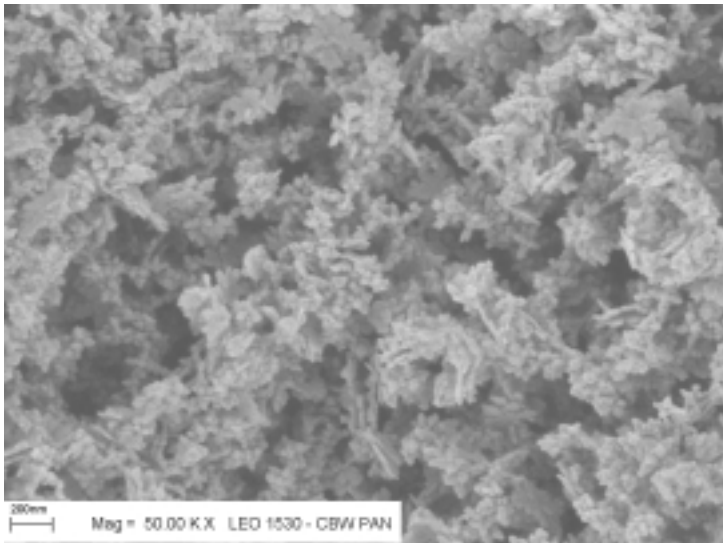

Figure 3. The SEM image (magnification – 50000 x) of the crystallites obtained from 6.52 at. % Co amalgam.

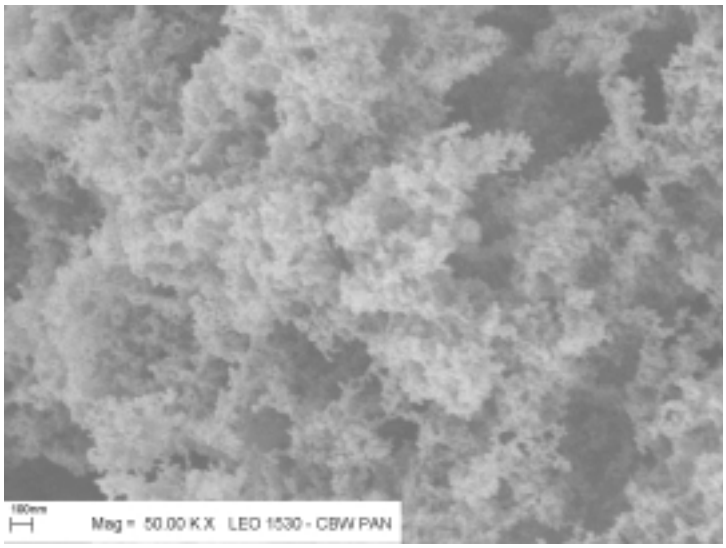

Figure 4. The SEM image (magnification – 50000 x) of the crystallites obtained from 1.36 at. % Co amalgam.

It can be seen from Figs. 3 and 4 that the cobalt nanocrystallites are fused and form aggregates having sizes of several or more microns. The agglomerates, shown in Fig. 3, seem to be formed from single grains, which have sizes in the range from 30 to 70 nm. Single grains have irregular shapes and are not spherical. In Fig. 4, the single grain size is remarkably smaller, *i.e.* less than 20 nm. We believe that such a difference in size of the nanocrystallites is associated with various cobalt contents in the

amalgams. It should be noted that the crystallites shown in Figs. 3 and 4 were prepared with the same concentration of Co ions in solution, but the number of aliquots of the solution was different in each case. In both experiments, the same stirring conditions were used.

The single grains (subunits) of Co crystallites are visible in more detail at higher magnifications in Figs. 5 and 6 for higher and lower concentrations of Co in amalgam, respectively.

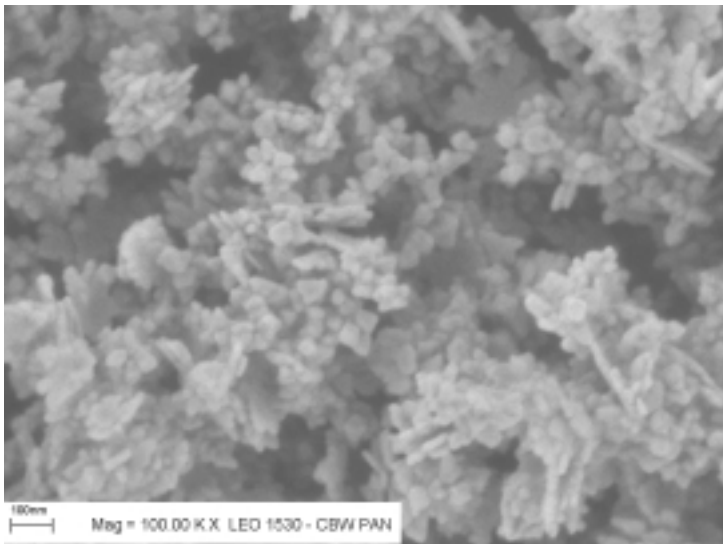

Figure 5. The SEM image (magnification – 100000 x) of the crystallites obtained from 6.52 at. % Co amalgam.

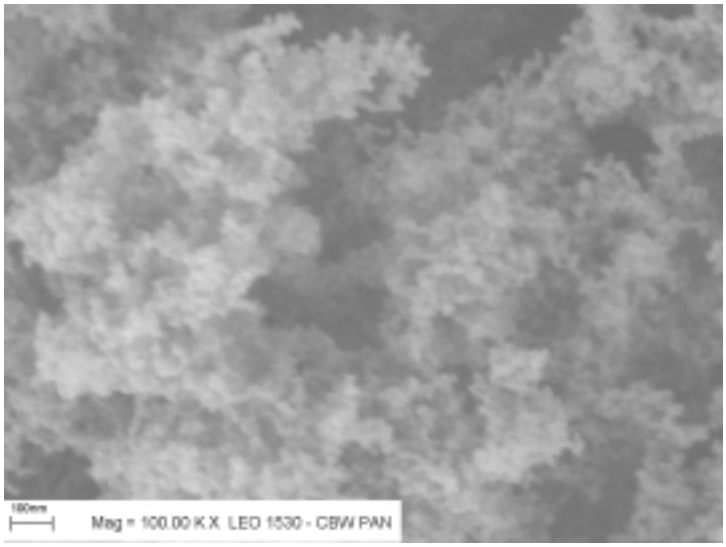

Figure 6. The SEM image (magnification – 100000 x) of the crystallites obtained from 1.36 at. % Co amalgam.

In conclusion, a black powder obtained from the amalgam consists of agglomerates, which can be observed under the electron microscope. The agglomerates have sizes in the range of microns and consist of nanometer-size grains, visible only at high magnification. The size of the grains depends on the method of amalgam preparation, especially on cobalt concentration. The results indicate that smaller grains are obtained with the lower cobalt concentration. The other experimental methods described below lead to the same conclusions. In BET analysis, the specific surface increases with the decrease of the cobalt concentration. The X-rays results suggest that the dimensions of monocrystals are in the range from 4 to 16 nm. The calculated sizes vary, depending on the face orientation, suggesting that the grains can be elongated in some directions. Such shapes as plates, and other similar shapes, far different from spherical, are also visible in high-resolution SEM images.

BET measurements. We used the BET analysis in order to determine the specific surface of the prepared crystallites. Prior to the measurements, all the samples were kept under vacuum for 90 min to remove adsorbed gases. All operations were performed at room temperature.

The results obtained for various cobalt samples, *i.e.* Cobalt 0, Cobalt 1 and Cobalt 2 have been summarized in Table 1. The results for platinum black are also presented in this table for the sake of comparison.

Table 1. Specific surface for different cobalt samples.

	Platinum black	Cobalt 0	Cobalt 1	Cobalt 2
Surface area [m^2/g]	**20.3**	**27.2**	**30.5**	**38.1**

The results of specific surface measurements using BET method are significantly different for cobalt samples prepared under various experimental conditions and vary between 27 and 38 m^2/g. These values are even higher than those obtained for platinum black (20.3 m^2/g). As expected, the samples having smaller grain size, as observed in electron microscope (Figs. 3–6), appear to have higher specific surfaces.

X-ray analysis. According to the results of the X-ray analysis, the analysed Co crystalline samples are not homogeneous. Three different species were identified: 1) hexagonal cobalt εCo (space group $P6_3/mmc$, a = 0.25071 nm and c = 0.40686 nm); 2) regular cobalt oxide Co_3O_4 (space group $Fd\bar{3}m$, a = 0.8084 nm) – maxima at 2θ about 39.47° and 47.06°; 3) regular cobalt oxide CoO (space group $Fm\bar{3}m$, a = 0.4260 nm) – maxima at 2θ about 46.30° and 53.96°.

The diffused diffraction maxima in different parts of spectrum (Fig. 7), especially when 2θ is close to 24°, may indicate that a phase with very small crystals is present in the sample. The fact that they appear, may also be associated with some small quantities of mercury present in the sample. The results of the EDX (energy dispersive X-ray) analysis confirmed that there is a small but detectable amount of mercury in the cobalt powder prepared from the amalgams (more than 0.2 at. % but less than 0.5 at. %).

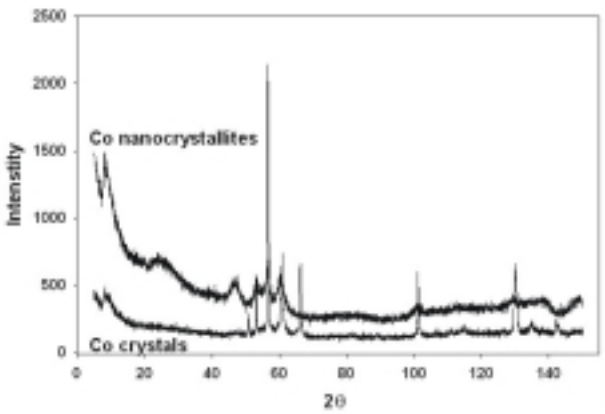

Figure 7. X-ray powder diffraction patterns of cobalt nanocrystallites and cobalt crystals.

This amount of mercury is probably adsorbed on the surface of the crystallites or occluded inside, because, according to Guminski [19], the solubility of Hg in solid Co is not higher than 0.01 at % Hg. So, the presence of mercury does not affect the calculations of the crystallites size.

The size of these crystals has been calculated from the diffractional line widths, according to the Scherrer equation:

$$B = 0.9\,\lambda/t\,\cos\theta \tag{1}$$

where: B is the line diffusion related to the crystallites size, in radians, t is the size of the crystallite, in nm and λ is the wavelength of the radiation equal to 0.19373 nm.

B can be estimated from the following equation:

$$B^2 = B_m^2 - B_s^2 \tag{2}$$

where: B_m is the width at half-height of the diffraction line for the investigated sample; and B_s is the width at half-height of the diffraction line for the reference sample in which the crystallite size is over 100 nm.

As a reference, the polycrystalline cobalt sample having crystal sizes between 0.1 and 10 μm was used. The results of the X-ray analysis of Cobalt 2 are summarized in Table 2.

Table 2. Grain sizes calculated from X-ray diffraction peaks identified in Fig. 7.

No	2θ [deg]	d_{exp} [nm]	d_{calc} [nm]	hkl	Phase	B_m [rad]	Grain size [nm]
1	53.15	0.2167	0.2171	100	εCo	0.0318 ± 0.010	6.2 ± 2.0
2	56.55	0.2045	0.2035	002	εCo	0.0157	15.2 ± 2.5
3	60.37	0.1926	0.1916	101	εCo	0.0485	4.2 ± 0.3
4	100.83	0.1257	0.1254	110	εCo	0.031 ± 0.011	9.2 ± 3.2
5	129.42	0.1071	0.1067	112	εCo	0.0686 ± 0.024	6.4 ± 2.3

The cobalt nanocrystallites obtained in this work consist of hexagonal ε Co, which is thermodynamically stable at temperatures below 420°C [5]. The crystallites are to some extent oxidized. The X-ray analysis indicates that some amount of cobalt oxides CoO and Co_3O_4 is present in the sample. This result is in agreement with the data presented by Bönnemann *et al*. [2] for small (10 nm in size) cobalt particles. However, in both their and our experiments, there is zerovalent cobalt present under the surface of the oxide layer.

We are still not sure whether the aggregation of Co nanocrystallites occurs during the growth of the grains in mercury, or after separation of both phases. The first possibility seems to be more probable, however, as relatively fast separation of cobalt from mercury may be explained by a large size of cobalt agglomerates already formed in mercury phase. One should also take into account the fact that the magnetic moments may be a strong agglomeration driving force.

It should be pointed out that Luborsky [15,16], Keeling *et al*. [17], and Windle *et al*. [7] in their publications did not explain clearly the aggregation mechanism. In particular, they did not predict the presence of the secondary structure of the Co nanocrystallites, visible on SEM images (Figs. 3–6) as small particles aggregated into larger structures. It seems that the crystallites are not obtained in the crystallization according to the diffusion-limited aggregation – DLA [20], *i.e*. they are not fractal, but they are rather built from subunits in at least a two-step process. We suggest that such growth of crystalline subunits can be explained by the burst-nucleation followed by aggregation, according to Reiss [21] and Park *et al.* [22] theory, developed to describe the growth of colloidal particles, *e.g*. gold, in aqueous solutions. It seems that this mechanism can also be useful for amalgams. In our case, the mechanism of growth of Co crystallites could consist of the following steps: (i) nucleation in supersaturated solution, (ii) growth of crystalline subunits (grains), (iii) agglomeration of the grains, (iv) further diffusional growth of the grains formed into clusters, (v) leaving the mercury phase due to the buoyancy effect.

In step (i) of the mechanism, the driving force is the supersaturation of a solute. As mentioned earlier in the Introduction, the equilibrium solubility of Co in Hg is extremely low. We can conclude, therefore, that directly after the reduction, a supersaturated cobalt amalgam is obtained, and then a burst-nucleation of metallic cobalt may occur. The burst-nucleation is a statistical process and it takes time to create a sufficient number of stable nuclei, which, by their growth, can effectively remove Co atoms from the mercury phase, decreasing its supersaturation.

If, however, the Co concentration in Hg is lowered, and also the temperature is decreased, then the rate of formation of stable Co nuclei is drastically lowered and the formation of a homogeneous amalgam can be observed. In fact, under such conditions and at short times of the experiment, the presence of a homogeneous cobalt amalgam has been detected in our previous work [11].

The explanation of the observed facts that the smaller concentration of Co in mercury leads to the smaller grains of the crystallites is not obvious. We think that this fact may, to some extent, result from the competition between the five processes,

discussed above. To confirm this hypothesis, it will be necessary to make some additional experiments and/or simulations. Very useful in the simulations may be some earlier observations done for example by Windle *et al*. [7] that after clustering the growth of the particles within the cluster is also possible.

CONCLUSIONS

Electrochemically prepared cobalt amalgam decomposes into a black cobalt powder. According to the analysis of the structure of the cobalt powder using SEM, specific surface measurements and X-ray diffraction, the powder consists of crystallites which are build of joined nanoparticles. The nanoparticles are not spherical and are partially oxidized. Their size depends on cobalt concentration in the amalgam and for 1.36 at. % cobalt amalgam is lower than 10 nm. Also, the specific surface of the nanocrystallites depends on cobalt concentration and reaches the value of 38.1 m^2/g for 1.36 at. % cobalt amalgam. Analysing the SEM images, we also came to the conclusion that the theory of particle growth in two steps, proposed by Park *et al*. [22] and used originally for colloidal particles in water, seems to be a novel and improved approach in a prediction of the kinetics of cobalt amalgam decomposition and the nanocrystallites growth as compared with the earlier approaches.

REFERENCES

1. Puntes V.F., Krishnan K. and Alivisatos A.P., *Top. Catal.*, **19**, 145 (2002).
2. Bönnemann H., Brijoux W., Brinkmann R., Matoussevitch N., Waldöfner N., Palina N. and Modrow H., *Inorg. Chim. Acta*, **350**, 617 (2003).
3. Matijevic E., *Faraday Discuss. Chem. Soc.*, **92**, 229 (1991).
4. Diehl M.R., Yu J.Y., Heath J.R., Held G.A., Doyle H., Sun S.H. and Murray C.B., *J. Phys. Chem. B*, **105**, 7913 (2001).
5. Gubin S.P. and Koksharov Yu.A., *Inorg. Mater.*, **38**, 1085 (2002).
6. Luborsky F.E., *J. Appl. Phys.*, **33**, 1909 (1962).
7. Windle P.L., Popplewell J. and Charles S.W., *IEEE Trans. Magn.*, **11**, 1367 (1975).
8. Mao L.C., Shan Z.Q., Yin S.H., Liu B. and Wu F., *J. Alloy Compd.*, **293**, 825 (1999).
9. Yuan A.B., Cheng S.A., Zhang J.Q. and Cao C.N., *J. Power Sources*, **77**, 178 (1999).
10. Galus Z., *CRC Crit. Rev. Anal. Chem.*, **4**, 359 (1975).
11. Paklepa P., Woroniecki J. and Wrona P.K., *J. Electroanal. Chem.*, **498**, 181 (2001).
12. Wrona P.K., *J. Electroanal. Chem.*, **197**, 395 (1986).
13. Ochodzki P. and Wrona P.K., *J. Electroanal. Chem.*, **277**, 225 (1990).
14. Galus Z., Guminski C., Balej J. and Salomon M., in: C. Hirayama, Z. Galus, C. Guminski (Eds.), Metals in Mercury: Solubility Data Series, vol. 25, Pergamon Press, Oxford, 1986.
15. Luborsky F.E., *J. Phys. Chem.*, **62**, 1131 (1958).
16. Luborsky F.E., *J. Phys. Chem.*, **61**, 1336 (1957).
17. Keeling L., Charles S.W. and Popplewell J., *J. Phys. F.*, **14**, 3093 (1984).
18. Falk R.B. and Luborsky F.E., *Trans. Metall. Soc. AIME*, **233**, 2079 (1965).
19. Guminski C., *J. Phase Equil.*, **14**, 643 (1993).
20. Witten T.A. and Sander L.M., *Phys. Rev. Lett.*, **47**, 1400 (1981).
21. Reiss H., *J. Chem. Phys.*, **19**, 482 (1951).
22. Park. J., Privman V. and E. Matijević, *J. Phys. Chem. B*, **105**, 11630 (2001).